Mon. Not. R. Astron. Soc. **317**, 658–666 (2000)

Relativistic beaming effects in the spectra of cores and hotspots in radio galaxies and quasars

C. H. Ishwara-Chandra[1,2,3]★ and D. J. Saikia[1]★

[1]*National Centre for Radio Astrophysics, TIFR, Post Bag 3, Ganeshkhind, Pune 411 007, India*
[2]*Joint Astronomy Programme, Department of Physics, Indian Institute of Science, Bangalore 560 012, India*
[3]*Raman Research Institute, Sadashiva Nagar, Bangalore 560 080, India*

Accepted 2000 May 2. Received 2000 January 31; in original form 1999 October 12

ABSTRACT

We present the results of multiwavelength observations of cores and hotspots, at *L*, *C*, *X* and *U* bands with the Very Large Array, of a matched sample of radio galaxies and quasars selected from the Molonglo Reference Catalogue. We use these observations to determine the spectra of cores and hotspots, and test the unified scheme for radio galaxies and quasars. Radio cores have been detected at all wavelengths in all of the quasars in our sample, whereas only ~50 per cent of the galaxies have cores detected in at least one of the wavelengths. The degree of core prominence in this sample is consistent with the unified scheme for radio galaxies and quasars. A comparison of the distributions of the two-point spectral index of the cores in our sample of lobe-dominated quasars, with the distributions in a matched sample of core-dominated quasars, shows that the distributions for these two classes are significantly different, and this is consistent with the expectations of the unified scheme. The difference in the spectral indices of the two hotspots on opposite sides is also significantly larger for quasars than for radio galaxies, as is expected in the unified scheme. We also investigate the relationship between the spectral index of the hotspots and the redshift or luminosity for our sample of sources.

Key words: galaxies: active – galaxies: nuclei – quasars: general – radio continuum: galaxies.

1 INTRODUCTION

In the orientation-based unified scheme for radio galaxies and quasars, these objects are believed to be intrinsically similar, but appear to be different because of their different orientations to the line of sight. The quasars are oriented close to the line of sight, whereas the radio galaxies lie close to the plane of the sky, with the dividing line being about 45°. There has been a reasonable degree of observational evidence in different wave bands in support of such a scheme (Scheuer 1987; Barthel 1989; Antonucci 1993; Urry & Padovani 1995).

In this paper we investigate the effects of relativistic beaming in the spectra of cores and hotspots in a matched sample of radio galaxies and quasars, in order to further test the unified scheme for these objects. We have attempted to determine the spectra of the cores using observations at two widely spaced *L*-band frequencies, and at *C*, *X* and *U* bands. These observations represent one of the more extensive studies on the spectra of relatively weak cores in lobe-dominated radio sources. In an earlier study, Athreya et al. (1997) found a high proportion of cores in their sample of high-redshift radio galaxies to have a steep radio spectrum between 4.7 and 8.3 GHz, and identified this with the optically thin part of the core spectrum. They also examined the spectra of core- and lobe-dominated quasars from available data in the literature, and suggested that the galaxy and quasar cores have intrinsically similar radio spectra. Lonsdale, Barthel & Miley (1993) found most of the radio cores in their sample of high-redshift, lobe-dominated quasars to have steep spectra between 5 and 15 GHz, indicating the presence of optically thin components. This is possibly a result of the high emitted frequencies corresponding to these sources. We present the spectra of the cores in our sample and examine the effects of relativistic beaming in Section 4.

Relativistic effects in the spectra of hotspots in radio galaxies and quasars selected from the 3CR sample have been examined recently by Dennett-Thorpe et al. (1997, 1999). For the quasars they find that the spectrum of the high-surface-brightness region is indeed flatter on the jet side, but that the spectrum of the low-brightness region is flatter on the side with the longer lobe. They interpret these results in terms of relativistic bulk motion in the spectra of the high brightness regions, and differential synchrotron ageing in the low-brightness regions. For the Fanaroff–Riley II

★ E-mail: ishwar@ncra.tifr.res.in (CHIC); djs@ncra.tifr.res.in (DJS)

(FRII) galaxies, the spectral asymmetries appear to be uncorrelated with jet sidedness at all brightness levels, but they do appear to be related to the relative lobe volume. In addition, earlier studies have shown that the less depolarized lobe has a flatter radio spectrum (Liu & Pooley 1991) and generally faces the radio jet (Garrington et al. 1988; Laing 1988; Garrington, Conway & Leahy 1991). We examine the effects of relativistic beaming in the spectra of the hotspots in our sample of radio galaxies and quasars using the scaled-array observations at *L*, *C* and *U* bands. These results are presented in Section 5. We also investigate any dependence of hotspot spectral indices on redshift or radio power.

In this paper, the sample and the observations are described in Section 2, and the observational results on the radio cores are presented in Section 3. The observed core prominence, the core spectra and their consistency with the unified scheme are presented in Section 4. The consistency of the hotspot spectra with the relativistic beaming effects and the unified scheme, as well as the dependence of hotspot spectra on redshift or luminosity, are discussed in Section 5. The conclusions are summarized in Section 6.

Table 1. Observing log.

Array Conf.	Obs. band	Obs. Freq. (MHz)	Band-width (MHz)	Date of obs.
BnA	*L*	1365	50	1995 September 20
	L	1665	25	
CnB	*C*	4635	50	1996 January 20, 31
	C	4935	50	
DnC	*U*	14 965	50	1997 September 15, 16
DnC	*U*	14 965	50	1997 October 3, 4, 12
BnA	*X*	8447	25	1997 February 3

2 SOURCE SAMPLE AND OBSERVATIONS

The sample and the selection criteria are discussed in detail in an earlier paper reporting the polarization properties of this well-defined sample of radio galaxies and quasars selected from the Molonglo Reference Catalogue (MRC) 1-Jy sample (cf. Ishwara-Chandra et. al 1998, hereafter referred to as IC98). Briefly, the sample consists of 15 quasars and 27 radio galaxies larger than about an arcminute in size with similar redshift, luminosity and projected linear size distributions. The observations were made with scaled arrays of the Very Large Array (VLA) of the National Radio Astronomy Observatory (NRAO) at 1.4 and 1.7 GHz (*L* band), 5 GHz (*C* band) and 15 GHz (*U* band) with resolutions of ∼5 arcsec, while observations at 8 GHz (*X* band) have a resolution of ∼1 arcsec. At 15 GHz, 14 quasars and 10 radio galaxies were observed, while at 8 GHz only those sources in the RA range 03^h to 13^h were observed because of scheduling constraints. The observing log is summarized in Table 1. All the data were calibrated and analysed using the NRAO AIPS package.

Table 2. Observed and derived parameters of the radio cores.

Source	Id	z	Flux density of the core						α_L^C	α_C^U	f_c	Notes
			1365 MHz	1665 MHz	4635 MHz	4935 MHz	8450 MHz	15000 MHz				
0017−207	Q	0.545	2.8[d]	2.8	2.2	2.1		1.2	0.25	0.51	0.017	
0058−229	Q	0.706	4.3[d]	3.8[d]	2.1	2.4		1.0	0.51	0.71	0.020	
0133−266	Q	1.53	14.1	13.2	16.6	16.8			−0.17		0.10	
0148−297	G	0.41	1.9		0.4			2.5			0.00060	N
0428−281	G	0.65			∼0.3	∼0.2	∼0.3				0.00074	N
0437−244	Q	0.84	16.9	15.2	12.8	12.5	10.5	4.4	0.21	0.92	0.089	
0454−220	Q	0.533	190.7	180.5	137.0	137.5	167.4	162.1	0.26	−0.15	0.26	
0551−226	G	0.8					0.4				0.0040	N
0938−205	G	0.371					0.6				0.0058	
0955−283	G	0.8				0.6	1.0				0.0042	
1022−250	G	0.34					∼0.3				0.0039	N core?
1023−226	G	0.586					0.4				0.0050	
1025−229	Q	0.309	11.9	10.0	10.2	10.2	9.9	7.9	0.07	0.22	0.09	
1026−202	G	0.566			0.7	0.7	0.6	0.7			0.0040	
1029−233	G	0.611		0.8	0.5	0.4	0.5		0.56		0.0036	
1052−272	Q	1.103	2.3	2.1	1.8	2.0	1.2	1.2	0.13	0.40	0.0098	
1107−218	G	1.5					∼0.3				0.0023	N core?
1126−290	G	0.41			1.9	1.7	1.4				0.0054	N
1226−297	Q	0.749	1.7	2.3	4.0	3.9	4.6	4.6	−0.61	−0.13	0.029	
1232−249	Q	0.352	17.5	14.7	11.2	10.6	10.0	8.2	0.34	0.25	0.023	
1247−290	Q	0.77	14.2[d]	11.4[d]	2.4	2.1	1.7	1.2	1.50	0.55	0.013	
1257−230	Q	1.109	16.2	16.4	15.4	15.0	10.1	8.1	0.06	0.55	0.055	
1358−214	G	0.5					0.6				0.0074	
2035−203	Q	0.516	34.7	38.1	40.0	38.7		29.7	−0.073	0.25	0.20	
2040−236	Q	0.704	119.1	116.4	91.7	90.3		74.3	0.22	0.18	0.740	
2118−266	G	0.343	27.2	28.6	51.6	51.8		47.5	−0.53	0.074	0.620	
2213−283	Q	0.946	38.3	40.7	54.2	54.1		56.7	−0.27	−0.04	0.19	
2311−222	G	0.434	2.4	1.6	1.9	1.7		1.1	0.11	0.43	0.0077	
2338−290	Q	0.446	30.4	31.9	40.4	40.8		64.5	−0.23	−0.40	0.40	

The images in the *X* and *U* bands were corrected for primary beam attenuation. The *U*-band images have been restored with the same resolutions as the *L*- and *C*-band images, which are listed in table 3 of IC98.

3 DETECTION OF RADIO CORES

All the quasars have radio cores detected at all wavelengths. In the case of radio galaxies, only two have cores reliably detected at all wavelengths, but many of them have weakly detected cores in at least one wavelength. Of the 27 radio galaxies, 14 of them have a core detected in at least one wavelength, only 5 of which have a core flux density greater than 1 mJy. These 14 include two possible cores that are weak features seen only in the *X*-band images close to the positions of the optical galaxies. The peak flux densities of cores have been used to minimize the contribution from nearby extended emission, and these values have been estimated using the AIPS task IMFIT. In the giant source 1025−229, the core flux densities have been estimated by fitting a Gaussian to both the core and the nearby jet-like component in the *L*-, *C*- and *U*-band images. All the core flux densities estimated from the Gaussian fits are similar to the values at the pixel of maximum brightness near the optical position. Only the cores that could be clearly identified in the images have been listed in Table 2, which is arranged as follows. Column 1: source name; column 2: optical identification where Q denotes a quasar and G a radio galaxy; column 3: redshift of the source; columns 4–9: peak flux densities of the cores at 1365, 1665, 4635, 4935, 8450 and 15 000 MHz in units of mJy. In a few cases the core flux density could be significantly overestimated as a result of extended diffuse emission in the vicinity of the core. These have been marked with a superscript *d*. Columns 10 and 11 list the spectral indices between *L* and *C* bands, and between *C* and *U* bands, where the spectral index, α, is defined as $S(\nu) \propto \nu^{-\alpha}$. The spectral indices have been estimated using linear least-squares fitting between the bands using the core flux densities at both the frequencies in the *L* and *C* bands. Cores with the superscript *d* have not been used. Column 12 gives the fraction of emission from the core at an emitted frequency of 8 GHz using the core spectral index determined from our observations and a spectral index of 1 for the extended emission. Column 13: 'N' indicates that there is a note on the source in the text, while 'core?' indicates a possible core. The positions of the optical objects have been listed by either McCarthy et al. (1996, hereafter referred to as M96), if it is a galaxy, or by Kapahi et al. (1998, hereafter referred to as K98), if it is a quasar. The typical errors in the position of optical objects are about 1.5 arcsec (M96) whereas for the quasars errors are about 0.5 arcsec (K98). The positions of the new radio cores, which are not listed in K98, are presented in Table 3.

Notes on individual sources.

(i) 0148−297: the core is relatively weak at 4635 MHz; its position is the same as that of the stronger core at 15 GHz, and also consistent with the one seen at 1365 MHz.

(ii) 0428−281: a weak radio core is detected in both the *C* bands as well as in the *X* band. The radio positions of the core are the same for all frequencies; but the core is about 5.9 arcsec from the optical position given by M96.

(iii) 0551−226: the radio core detected in the *X* band is about 2.9 arcsec from the optical position listed by M96.

(iv) 1022−250: the possible radio core is about 2.1 arcsec from the position of the optical galaxy given by M96.

Table 3. Positions of radio cores.

Source	RA (B1950)	Dec. (B1950)
0148−297	$01^h\ 48^m\ 19\overset{s}{.}679$	$-29°\ 46'\ 45\overset{''}{.}00$
0428−281	$04^h\ 28^m\ 17\overset{s}{.}326$	$-28°\ 07'\ 11\overset{''}{.}20$
0551−226	$05^h\ 51^m\ 17\overset{s}{.}431$	$-22°\ 40'\ 18\overset{''}{.}50$
0938−205	$09^h\ 38^m\ 30\overset{s}{.}873$	$-20°\ 33'\ 46\overset{''}{.}60$
0955−283	$09^h\ 55^m\ 36\overset{s}{.}536$	$-28°\ 23'\ 45\overset{''}{.}60$
1022−250	$10^h\ 22^m\ 57\overset{s}{.}085$	$-25°\ 01'\ 08\overset{''}{.}00$
1023−226	$10^h\ 23^m\ 10\overset{s}{.}267$	$-22°\ 38'\ 07\overset{''}{.}00$
1026−202	$10^h\ 26^m\ 35\overset{s}{.}174$	$-20°\ 12'\ 04\overset{''}{.}20$
1029−233	$10^h\ 29^m\ 12\overset{s}{.}174$	$-23°\ 23'\ 56\overset{''}{.}00$
1107−218	$11^h\ 07^m\ 44\overset{s}{.}986$	$-21°\ 51'\ 13\overset{''}{.}40$
1126−290	$11^h\ 26^m\ 26\overset{s}{.}443$	$-29°\ 05'\ 02\overset{''}{.}40$
1358−214	$13^h\ 58^m\ 47\overset{s}{.}273$	$-21°\ 27'\ 40\overset{''}{.}40$

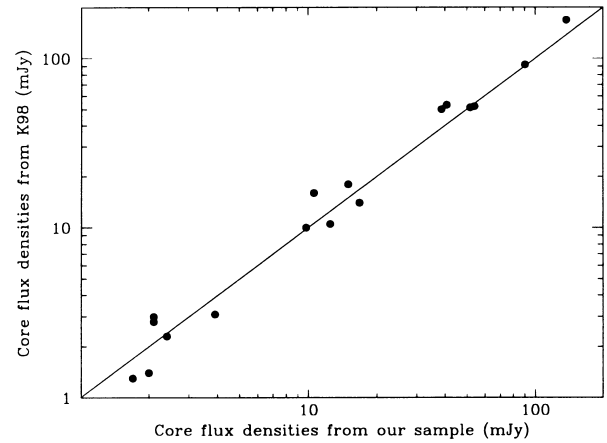

Figure 1. Plot of core flux densities at 4.9 GHz from K98 against the values estimated from our observations. Our estimates of core flux densities are from observations with an angular resolution of ∼5 arcsec compared with an accuracy of ∼1 arcsec for K98.

(v) 1107−218: the possible radio core is about 1.6 arcsec from the position of the optical galaxy given by M96.

(vi) 1126−290: the positions of the core in both the *C* bands and in the *X* band are consistent, but the core is about 12.4 arcsec from the optical position given by M96. The position of the centroid of the optical galaxy measured from recent CCD observations of the field is RA $11^h\ 26^m\ 26\overset{s}{.}434$ and Dec. $-29°\ 05'\ 02\overset{''}{.}74$ in B1950 coordinates. This is close to the position of the radio core.

4 RELATIVISTIC BEAMING IN THE CORES

To examine the consistency of the observations with the expectations of the unified scheme, one needs to estimate reliably the flux density of the cores at the different frequencies. As our observations at all the frequencies, except at 8 GHz, have been made with coarser angular resolution than is desirable, we have compared our measurements at 5 GHz with those of K98, which were also made at about 5 GHz but with an angular resolution of about 1 arcsec. The data are plotted in Fig. 1 for all the objects in our sample for which core flux densities have been listed by K98. As the epochs of the observations are separated by about 5–10 yr, there could be differences resulting from variability of the core

flux density. It is, however, clear from the figure that the values are consistent over a wide range of flux density. Besides suggesting that the cores might be only weakly variable, this also suggests that the effect of the coarser resolution is not significant at 5 GHz. In the *U* band it is likely to be even less significant, whereas in the *L* band we have identified the measurements that are likely to be significantly affected by diffuse emission in the vicinity of the cores.

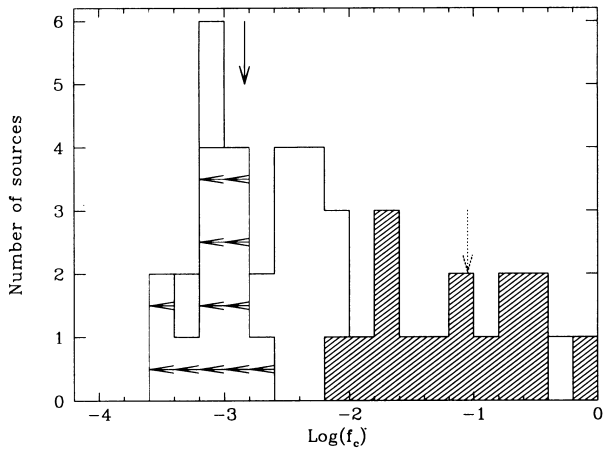

Figure 2. Distributions of f_c, the fraction of emission from the core at an emitted frequency of 8 GHz, for the Molonglo radio galaxies and quasars in our sample. The quasars are shown by the hatched area with the upper limits indicated by horizontal arrows. The median values of f_c for radio galaxies and quasars are shown by vertical solid and dotted arrows respectively.

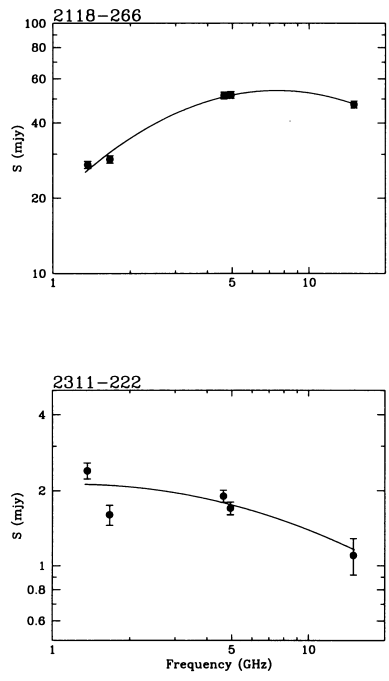

Figure 3. Observed spectra of two radio galaxy cores. The *x*-axis represents the frequency in GHz and the *y*-axis represents the flux density in mJy. The source names are given in the top-left corner of each spectrum. The details of the fitted curves are described in the text.

4.1 Core prominence

In the orientation-based unified scheme for radio galaxies and quasars, the quasars are expected to show more prominent cores than radio galaxies because of the effects of relativistic beaming. All quasars have detected cores, compared with about 50 per cent for the radio galaxies. The distributions of f_c, the fraction of emission from the core at an emitted frequency of 8 GHz, for our sample of radio galaxies and quasars is shown in Fig. 2. The median values of the f_c are about 0.09 ± 0.04 for quasars and less than about 0.0015 ± 0.02 for the radio galaxies. Given the statistical uncertainties resulting from the small size of the sample, these values are consistent with earlier estimates for the 3CR sample (cf. Saikia & Kulkarni 1994) as well as for a larger sample of Molonglo objects (K98). These values are consistent with the unified scheme for radio galaxies and quasars.

4.2 Spectra of cores

As only two of the galaxies have cores detected at all the observed wavelengths, to determine reliably the spectra of the cores (Fig. 3), we concentrate on the core spectra of the quasars to examine the effects of relativistic beaming. The spectra of all the cores in quasars are presented in Fig. 4. In both the figures, the error bars correspond to a 3 per cent error on absolute flux density calibration and 1σ noise in the image. The spectra have been fitted by either a two- or three-degree polynomial, and in one source, 0454−220, by a straight line and a two-degree polynomial. The spectra are usually complex. The steep low-frequency spectra in the quasars 0058−229 and 1247−290 are possibly a result of contributions from more extended emission near the core. The core in 1226−297 is a candidate Gigahertz Peaked Spectrum (GPS) source (cf. O'Dea 1998) with a turnover frequency around 15 GHz, but higher frequency measurements would be required to confirm this.

In the observed spectra of the cores, the rest frequency in the frame of the quasar will appear shifted as a consequence of both the cosmological redshift and the Doppler shift arising from the relativistic beaming of the nuclear or core emission. The rest frequency will be shifted by an amount $\delta/(1+z)$, where $\delta = [\gamma(1-\beta\cos\theta)]^{-1}$ is the Doppler factor, z the redshift of the source, γ the Lorentz factor, $\beta = v/c$ and θ is the angle of inclination of the jet or source axis to the line of sight. For fixed observed frequencies, ν_1 and ν_2, the spectrum will be blueshifted for quasars, and in case of radio galaxies it will be generally redshifted. Assuming a Lorentz factor of 5, the Doppler factor δ for inclination angles of 15°, 30° and 60°, which correspond roughly to orientations of core-dominated quasars (CDQs), lobe-dominated quasars (LDQs) and radio galaxies, are 3.7, 1.3 and 0.4 respectively. As we have determined the spectra of only two cores in radio galaxies, we concentrate on the quasars and compare their spectra with a sample of core-dominated quasars that have been observed at a single epoch by Saikia et al. (1998). The two samples have similar redshift distributions and have similar extended radio luminosity within a factor of ∼2. We present the distributions of the spectral index between 1.4 and 5 GHz (α_C^L) and the distributions between 5 and 15 GHz (α_U^C) for both the samples of LDQs and CDQs in Fig. 5. These show that both α_C^L and α_U^C for CDQs are flatter compared with the corresponding values for LDQs, and the effect is more prominent in the high-frequency spectral index value (α_U^C). The median value of the two-point spectral index between 1.4 and 5 GHz, and that between 5 and

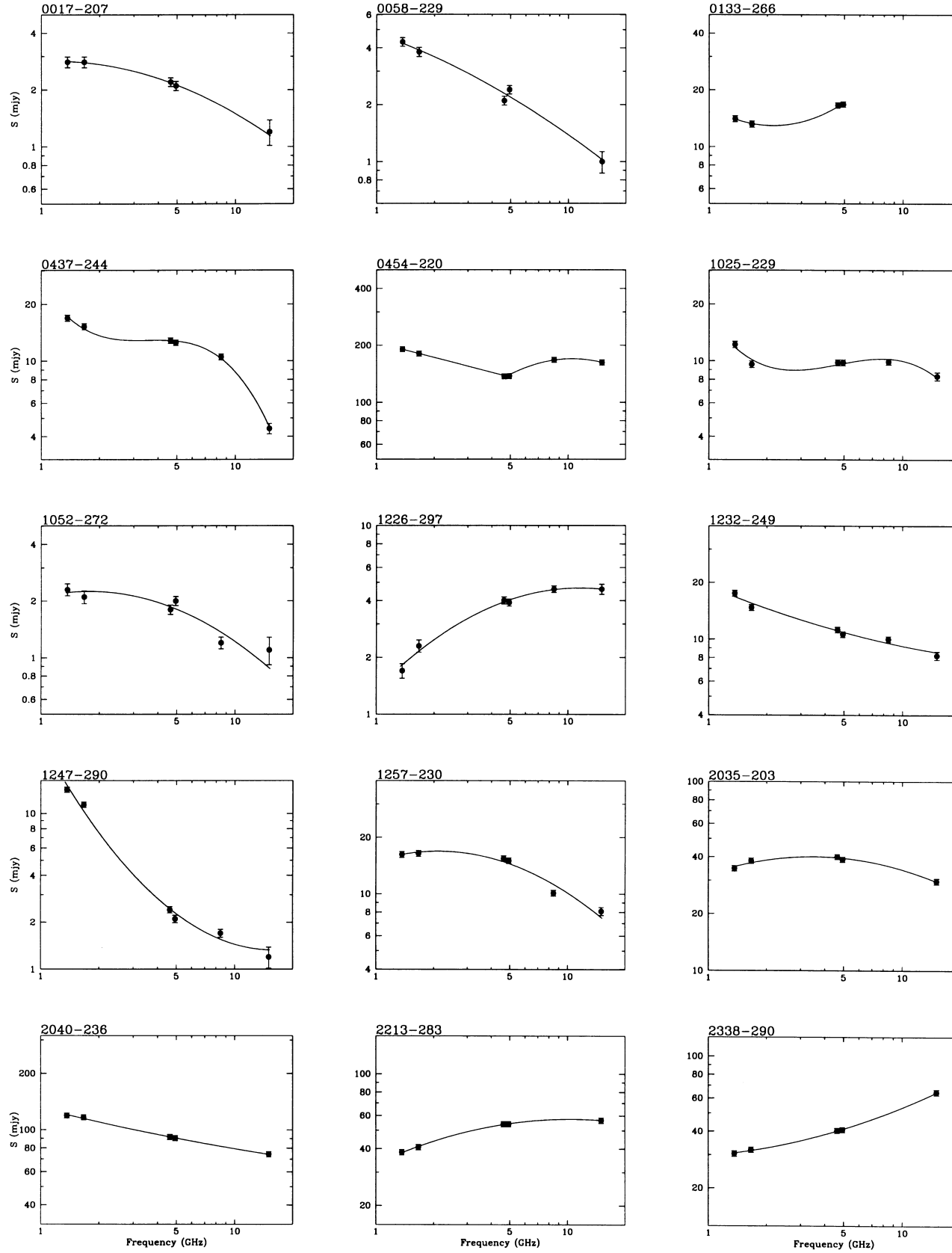

Figure 4. Observed radio spectra of quasar cores. The *x*-axis represents the frequency in GHz and the *y*-axis represents the flux density in mJy. The source names are given in the top-left corner of each spectrum. The details of the fitted curves are described in the text.

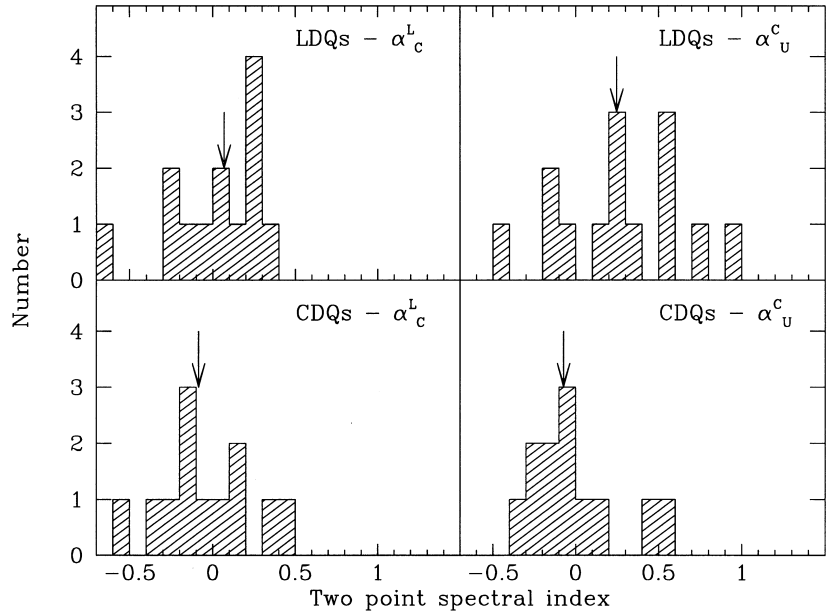

Figure 5. Comparison of the two-point spectral indices of lobe-dominated (LDQs) and core-dominated quasars (CDQs). The distributions of the spectral index between the *L* and *C* bands and between the *C* and *U* bands are shown in the left-hand and right-hand panels, respectively. The median values of each distribution are shown by arrows.

15 GHz, for LDQs are 0.07 ± 0.074, and 0.25 ± 0.085, respectively, while the corresponding values for the CDQs are -0.085 ± 0.073 and -0.073 ± 0.068, respectively. A Kolmogorov–Smirnov test shows that the distributions of α_U^C for LDQs and CDQs are different at a >99 per cent significance level, while the distributions of α_C^L are different at less than about the 80 per cent significance level. These trends are consistent with the unified scheme because the spectra of CDQs will be blueshifted by a larger amount than LDQs as a result of relativistic beaming. The trend is more prominent at the higher frequency, possibly as a consequence of the observed frequency often being closer to the optically thin region of the synchrotron spectrum.

5 RELATIVISTIC MOTION IN THE HOTSPOTS

Estimates of hotspot advance speeds made from attributing arm-length asymmetries to geometrical projection and light-travel time effects range from about 0.2–0.5*c* (e.g. Longair & Riley 1979; Banhatti 1980; Best et al. 1995). Tighter constraints have been placed by Scheuer (1995) by noting that the approaching side can be identified in sources with radio jets (cf. Saikia 1981). He estimates an upper limit of $\sim 0.1c$. The properties of highly asymmetric or completely one-sided radio sources indicate hotspot advance speeds in the range of ~ 0.2–$0.8c$ (Saikia et al. 1990). Proper motion studies of hotspots in compact very long baseline interferometry scale double radio sources yield values from about 0.05–0.5*c* (cf. O'Dea 1998).

5.1 Effects of relativistic motion in hotspot spectra

Assuming that the hotspots are advancing at mildly relativistic speeds, the observed spectral indices of the oppositely directed hotspots might appear to be different as a result of relativistic motion. If the hotspot spectra steepen towards higher frequencies,

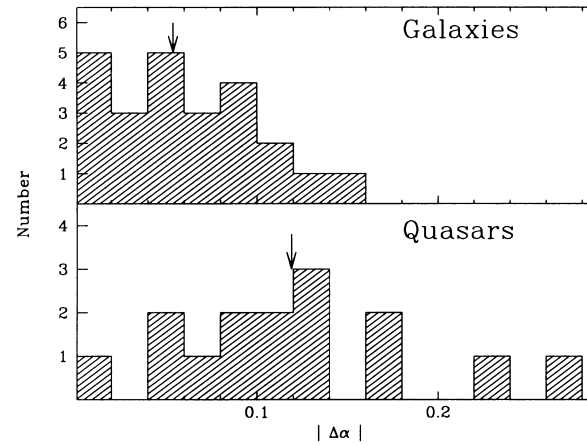

Figure 6. The distributions of the absolute difference in the hotspot spectral index $|\Delta\alpha|$ between 1.4 and 5 GHz for the radio galaxies and quasars. The arrows indicate the median values.

the approaching hotspot should exhibit a flatter spectrum over a fixed observed frequency range compared with the receding one because of relativistic Doppler effects. If the spectra are straight, any observed difference will reflect intrinsic differences in their spectra.

In the unified scheme for radio galaxies and quasars, the latter should exhibit a larger difference in the spectral indices of the hotspots on opposite sides as a consequence of the smaller angles of inclination to the line of sight. Assuming a canonical spectrum for the hotspot, one might also be able to estimate the hotspot advance speeds for a sample of sources from the observed difference in hotspot spectral indices. For sources with detected radio jets, one can identify the approaching and receding hotspot. However, because we do not have radio jets detected in almost all of the sources in our sample, we attempt such a study by examining the absolute difference in the hotspot spectral indices of the oppositely directed hotspots for the radio galaxies and

quasars. In our study, we have defined the hotspot as the peak pixel in each lobe with a surface brightness at least 10 times the value of the weakest reliable flux density level. The number of sources with reliable hotspot flux densities in the *U* band are small. Therefore, we concentrate on the *L*- and *C*-band observations, but also check for consistency with the *U*-band observations.

Our samples of radio galaxies and quasars are of similar redshift and luminosity, and therefore the effects of cosmological redshift are similar. The distributions of the absolute difference in the hotspot spectral index $|\Delta\alpha|$ between 1.4 and 5 GHz is shown in Fig. 6. There is a clear tendency for the quasars to show a larger spectral index difference than radio galaxies. The median values of $|\Delta\alpha|$ are about 0.055 ± 0.0072 and 0.12 ± 0.015 for the radio galaxies and quasars respectively. A Kolmogorov–Smirnov test shows that the distributions are different at a >99 per cent significance level. The corresponding values for the spectral indices between *C*- and *U*-bands are 0.10 ± 0.015 and 0.19 ± 0.07 for the radio galaxies and quasars, again consistent with the trend expected in the unified scheme.

To understand the above difference in terms of relativistic beaming, we have considered a model hotspot spectrum with a curvature of 0.2 in the spectral index between each of the following successive pairs of frequencies, namely 0.408, 1.4, 5 and 15 GHz. There has been evidence in the past for curvature in the hotspot spectra. For example, Carilli et al. (1991) observed Cygnus A with an angular resolution of about 4.5 arcsec over a large frequency range and find evidence of spectral curvature in the hotspots. Wright, Chernin & Forster (1997) observed the hotspots in Cygnus A with an angular resolution of about 0.4 arcsec and also find evidence of spectral steepening (see also Section 5.2 of this paper). The flatter spectra of the hotspots on the jet side can be better explained if the intrinsic spectra are curved downwards towards higher frequencies (Dennett-Thorpe at al. 1997, 1999). Assuming the above spectrum and an angle of 30–50° for quasars and 50–90° for radio galaxies, hotspot advance speeds in the range of $\sim$0.2–0.5*c* are required to produce the observed difference in the distributions. However, with our angular resolution of about 5 arcsec, the corresponding sizes are typically about 25 kpc, which is significantly larger than the sizes of hotspots in FRII radio sources (cf. Bridle et al. 1994; Fernini, Burns & Perley 1997; Hardcastle et al. 1998; Jeyakumar & Saikia 2000). As the spectra of the extended emission tend to be steeper than the hotspots themselves, and the effects of relativistic beaming of hotspots are significant for quasars (Dennett-Thorpe at al. 1997, 1999), the relative contribution of the extended emission to our hotspot flux density within the 5-arcsec beam would tend to be larger for the receding hotspot compared with the flux density of the approaching one. This would tend to increase the apparent difference in the spectral indices of the oppositely directed hotspots, leading to a larger estimate of the hotspot velocity. Therefore, while our present estimates of $\sim$0.2–0.5*c* should be considered to be upper limits, a similar technique applied to higher resolution observations of hotspots should yield more reliable estimates of hotspot speeds. From our study the hotspot speeds appear to be, at most, mildly relativistic. It would also be important to study the curvature in the intrinsic spectra of the hotspots from higher resolution observations.

If the sources are intrinsically symmetric and the effects of evolution of individual components with age are not dominant, one would expect the approaching hotspot, which has a flatter spectral index, to be farther from the nucleus and also brighter. However, we have shown in our earlier paper (IC98) that most of these sources appear to be evolving in an asymmetric environment. Nevertheless, for quasars where the effects of orientation are likely to be more significant, we do find a weak trend for the flatter hotspot to be on the longer side. This is true for nine of the 14 quasars when one considers the spectral index between the *L* and *C* bands, and seven of the eight quasars for hotspot spectral indices between the *C* and *U* bands. The galaxies do not show any trend. We have also examined the relationship of the hotspot spectral indices with hotspot brightness ratio, but do not find any trend, possibly because of the effects of environment as well as the evolution of the individual components with age.

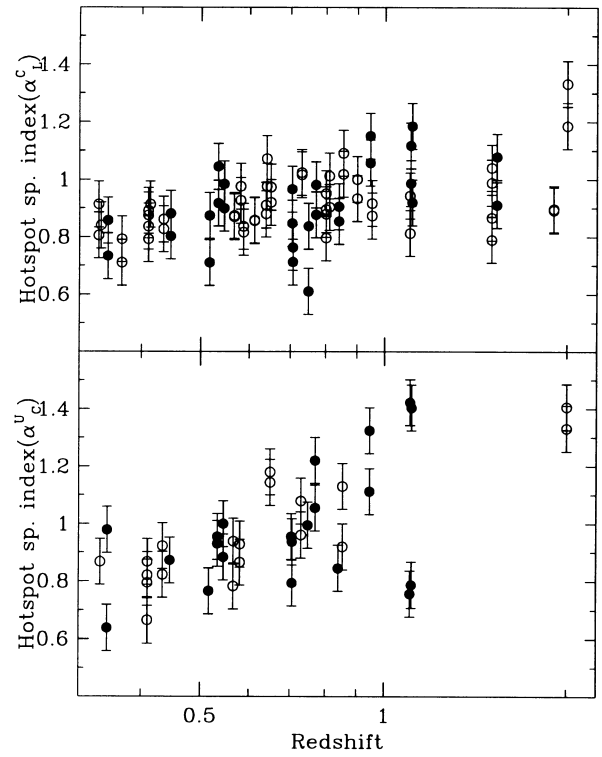

Figure 7. Plot of the hotspot spectral index against the source redshift. The *y*-axis represents the hotspot spectral index between 1.4 and 5 GHz (upper panel) and between 5 and 15 GHz (lower panel). Filled and open circles represent quasars and radio galaxies respectively.

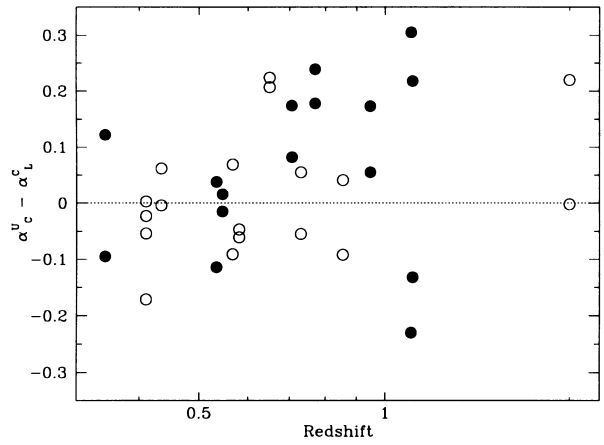

Figure 8. Plot of the difference of hotspot spectral index between 5 and 15 GHz and that between 1.4 and 5 GHz against the source redshift. Filled and open circles represent quasars and radio galaxies respectively.

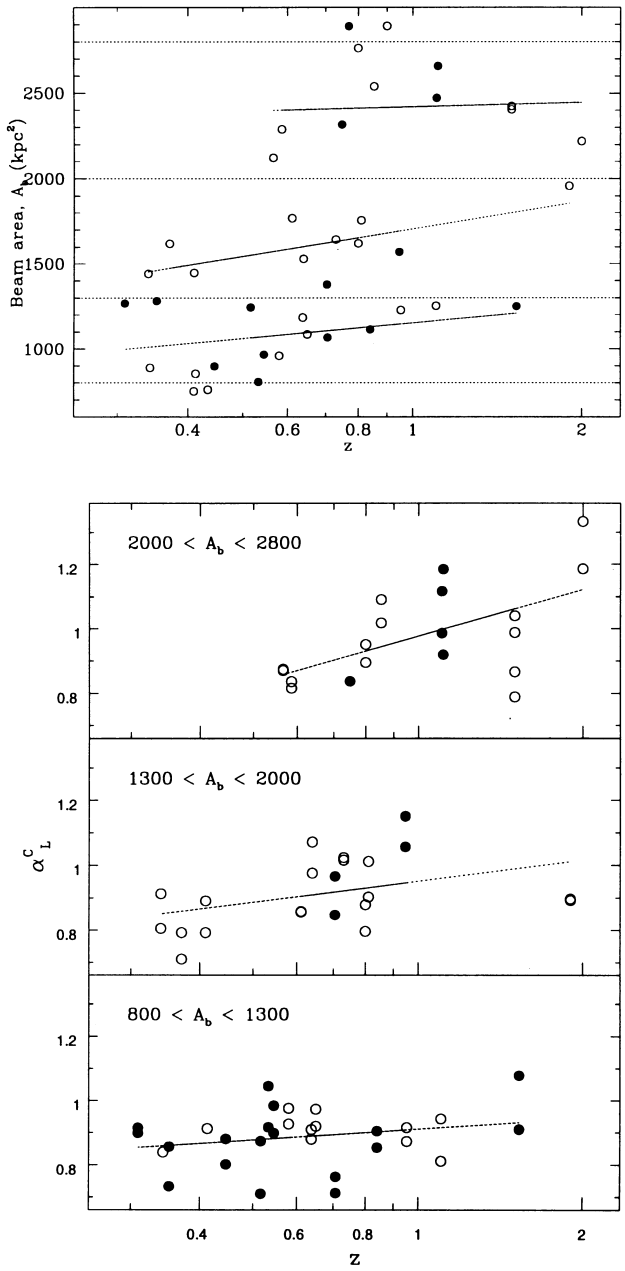

Figure 9. The area of the restoring beam A_b, in units of kpc^2, plotted against redshift for all the sources (upper figure). The hotspot spectral indices between *L* and *C* bands are plotted against redshift for sources in the three restricted ranges of beam area marked in the upper figure. The ranges of A_b are labelled in each plot. The dashed lines indicate least-squares fits to the data. Filled and open circles represent quasars and radio galaxies, respectively.

5.2 Spectral index–redshift/luminosity relationship for hotspots

We have examined the spectral index–redshift/luminosity relationship for our sample using the spectra of the hotspots. At a first glance, there appears to be a significant correlation of the spectral indices α_{hs} between 1.4 and 5 GHz, as well as between 5 and 15 GHz, with redshift z, the relationship being steeper for the higher frequency spectral index (Fig. 7). A Spearman rank correlation test shows the relationship to be significant at a level of >99 per cent. As our sources are from a flux-density-limited sample, redshift and luminosity are strongly correlated and we cannot distinguish between a dependence on either luminosity or redshift.

Steepening in the hotspot spectra towards higher frequencies because of radiative losses can, in principle, cause such a relationship as the emitted frequency will be higher for the higher redshift, and hence more luminous, objects. Inverse-Compton losses would also be important at higher redshifts. In a flux density limited sample, increased magnetic field for the more luminous objects will also increase the synchrotron emissivity, leading to an increase in the rate at which spectral steepening occurs (cf. Laing & Peacock 1980; Gopal-Krishna & Wiita 1990; Krolik & Chen 1991; Blundell, Rawlings & Willott 1999). Considering all the objects with $z < 1$, where the relationship is better defined, and dividing them into two equal groups in redshift, the median values of $\alpha_C^U - \alpha_L^C$ are about 0 and 0.06. There is a weak trend for the high-frequency spectra to be steeper than the low-frequency ones as one moves towards higher redshifts up to $z \sim 1$ (Fig. 8). Although we have plotted the observed spectral indices, rather the ones in the rest frame of the source, the median redshift of the objects with $z < 1$ is about 0.6, so that the emitted frequencies for the low-frequency spectral index is about 2.2 and 7.8 GHz. The median values of α_L^C increase from about 0.8 to 1 as the redshift increases from about 0.3 to 1. This range is larger than the observed degree of spectral curvature, indicating that the correlation is not merely a result of *K*-correction factors alone. This is consistent with earlier suggestions for the α–P relationship using the integrated spectra of the sources (cf. Lacy et al. 1993; van Breugel & McCarthy 1989).

However, while investigating the α–z relationship for hotspots one needs to consider the linear resolutions of the observations, which are likely to be coarser at higher redshifts leading to increased lobe contamination with increasing redshift. We have plotted the physical area of the restoring beam, A_b, for each source as a function of redshift, and have examined the α_{hs}–z relationship for sources in restricted ranges of A_b as shown in Fig. 9. We first consider the spectral indices between *L* and *C* bands where there are a larger number of sources. The slopes of the α_{hs}–z relationship for sources with $800 < A_b < 1300$, $1300 < A_b < 2000$ and $2000 < A_b < 2800$ kpc^2 are 0.11 ± 0.08, 0.21 ± 0.11 and 0.48 ± 0.16, respectively. For sources observed with the highest linear resolution, which has the minimum contamination from the extended emission, the α_{hs}–z plot is relatively flat, whereas the slope increases for sources observed with larger physical beam areas. A similar trend is seen when considering the hotspot spectral indices between the *C* and *U* bands. The slopes of the α_{hs}–z plot for the three ranges of beam areas are 0.47 ± 0.30, 0.99 ± 0.26 and 0.90 ± 0.39, respectively, the errors being larger because of the smaller number of sources observed in the *U* band. These trends suggest that the hotspot spectral indices, which are closely related to the injection spectrum, are at best weakly dependent on redshift, whereas the observed relationship is largely a consequence of the well-known relationship for the extended emission. It would be relevant to investigate the α_{hs}–z relationship with higher linear resolution than has been possible from our observations.

6 CONCLUDING REMARKS

We have studied multifrequency radio spectra of cores and

hotspots of a matched sample of radio galaxies and quasars. A comparison of the spectral indices of the cores of lobe-dominated and core-dominated quasars shows that the high-frequency spectral index of these two classes are significantly different. The difference can be understood in terms of Doppler effects and is consistent with the basic ideas of the unified scheme for radio galaxies and quasars.

The difference in the spectral indices of the hotspots on opposite sides of the nucleus is larger for quasars compared with radio galaxies, the median values of the difference being about 0.12 and 0.06, respectively. This difference could also be understood in terms of mild relativistic beaming of the hotspots. The hotspots have a curved radio spectrum steepening towards higher frequencies, possibly as a result of radiative losses. The difference is consistent with the unified scheme for radio galaxies and quasars and yields the velocity of advancement of the hotspots to be, at most, mildly relativistic.

We have investigated the correlation between spectral index and redshift/luminosity for the hotspots in our sample of sources. Although there appears to be a significant correlation, one needs to understand the effects of spectral steepening and lobe contamination in the hotspot spectral indices. Examining the low- and high-frequency spectral indices of the hotspots in our sample, the observed correlation cannot be caused by the effects of *K*-correction alone. However, considering sources observed with similar linear resolutions in terms of beam areas, reveals that the $\alpha_{\rm hs}$–z relationship is flatter for the ones observed with the highest linear resolutions compared with the ones observed with coarser resolution. The hotspot spectral indices depend, at best, marginally on redshift for those observed with the highest linear resolutions, whereas for those observed with coarser linear resolutions, the relationship appears similar to the well-known correlation for the extended emission. It would be interesting to investigate the spectral index–redshift relationship for hotspots using higher linear resolution than has been possible from our observations.

ACKNOWLEDGMENTS

We thank N. D. Ramesh Bhat, K. S. Dwarakanath, Gopal-Krishna, Vasant Kulkarni and Paul Wiita for their comments on the manuscript, and Ramesh Bhat for computational help. We are also indebted to an anonymous referee for very helpful and critical comments on the paper. The National Radio Astronomy Observatory is a facility of the National Science Foundation operated under cooperative agreement by Associated Universities Inc. We thank the staff of the Very Large Array for the observations.

REFERENCES

Antonucci R., 1993, ARA&A, 31, 473
Athreya R. M., Kapahi V. K., McCarthy P. J., van Breugel W., 1997, MNRAS, 289, 525
Banhatti D. G., 1980, A&A, 84, 112
Barthel P. D., 1989, ApJ, 336, 606
Best P. N., Bailer D. M., Longair M. S., Riley J. M., 1995, MNRAS, 275, 1171
Blundell K. M., Rawlings S., Willott C. J., 1999, AJ, 117, 677
Bridle A. H., Hough D. H., Lonsdale C. J., Burns J. O., Laing R. A., 1994, AJ, 108, 766
Carilli C. L., Perley R. A., Dreher J. W., Leahy J. P., 1991, ApJ, 383, 554
Dennett-Thorpe J., Bridle A. H., Scheuer P. A. G., Laing R. A., Leahy J. P., 1997, MNRAS, 289, 753
Dennett-Thorpe J., Bridle A. H., Laing R. A., Scheuer P. A. G., 1999, MNRAS, 304, 271
Fernini I., Burns J. O., Perley R. A., 1997, AJ, 114, 2292
Garrington S. T., Conway R. G., Leahy J. P., 1991, MNRAS, 250, 171
Garrington S. T., Leahy J. P., Conway R. G., Laing R. A., 1988, Nat, 331, 147
Gopal-Krishna Wiita P. J., 1990, A&A, 236, 305
Hardcastle M. J., Alexander P., Pooley G. G., Riley J. M., 1998, MNRAS, 296, 445
Ishwara-Chandra C. H., Saikia D. J., Kapahi V. K., McCarthy P. J., 1998, MNRAS, 300, 269 (IC98)
Jeyakumar S., Saikia D. J., 2000, MNRAS, 311, 397
Kapahi V. K., Athreya R. M., Subrahmanya C. R., Baker J. C., Hunstead R. W., McCarthy P. J., van Breugel W., 1998, ApJS, 118, 327 (K98)
Krolik J. H., Chen W., 1991, AJ, 102, 1659
Lacy M., Hill G. J., Kaiser M.-E., Rawlings S., 1993, MNRAS, 263, 707
Laing R. A., 1988, Nat, 331, 149
Laing R. A., Peacock J. A., 1980, MNRAS, 190, 903
Liu R., Pooley G. G., 1991, MNRAS, 249, 343
Longair M. S., Riley J. M., 1979, MNRAS, 188, 625
Lonsdale C. J., Barthel P. D., Miley G. K., 1993, ApJS, 87, 63
McCarthy P. J., Kapahi V. K., van Breugel W., Persson S. E., Athreya R. M., Subrahmanya C. R., 1996, ApJS, 107, 19 (M96)
O'Dea C. P., 1998, PASP, 110, 49
Saikia D. J., 1981, MNRAS, 197, 11P
Saikia D. J., Kulkarni V. K., 1994, MNRAS, 270, 897
Saikia D. J., Junor W., Cornwell T. J., Muxlow T. W. B., Shastri P., 1990, MNRAS, 245, 408
Saikia D. J., Holmes G. F., Kulkarni A. R., Salter C. J., Garrington S. T., 1998, MNRAS, 298, 877
Scheuer P. A. G., 1987, in Zensus J. A., Pearson T. J., eds, Superluminal Radio Sources. Cambridge Univ. Press, Cambridge, p. 104
Scheuer P. A. G., 1995, MNRAS, 277, 331
Urry C. M., Padovani P., 1995, PASP, 107, 803
van Breugel W., McCarthy P. J., 1989, in Meurs E. J. A., Fosbury R. A. E., eds, Extranuclear activity in galaxies. ESO Conf. Workshop Proc. 32. ESO, Germany, p. 227
Wright M. C. H., Chernin L. M., Forster J. R., 1997, ApJ, 483, 783

This paper has been typeset from a TEX/LATEX file prepared by the author.